




Single-Polarization and Single-Mode Hybrid Hollow-Core Anti-Resonant Fiber Design at $2 \mu\text{m}$

Herschel Herring , Mohammad Al Mahfuz , *Member, IEEE*, and Md. Selim Habib , *Senior Member, IEEE*

Abstract—In this paper, to the best of our knowledge, a new type of hollow-core anti-resonant fiber (HC-ARF) design using hybrid silica/high-index material (HIM) cladding is presented for single-polarization, high-birefringence, and endlessly single-mode operation at $2 \mu\text{m}$ wavelength. We show that the inclusion of a HIM layer in the cladding allows strong suppression of x -polarization, while maintaining low propagation loss and single-mode propagation for y -polarization. The optimized HC-ARF design includes a combination of low propagation loss, high-birefringence, and polarization-extinction ratio (PER) or loss ratio of 0.02 dB/m, 1.2×10^{-4} , and >550 respectively, while the loss of the x -polarization is >20 dB/m. The proposed fiber may also be coiled to small bend radii while maintaining low bend-loss of ≈ 0.01 – 0.1 dB/m, and can potentially be used as polarization filter based on the different gap separations and bend conditions.

Index Terms—Hollow-core anti-resonant fiber, high-birefringence, single-polarization, single-mode fiber.

I. INTRODUCTION

THE $2 \mu\text{m}$ wavelength is of particular interest in the field of optics and photonics due to its unique property of high absorption in water. This characteristic allows for an enormous range of optical fiber system applications such as biomarker detection, environmental observation, and molecular spectroscopy [1], [2]. High light transmission, high-birefringence and excellent polarization control [3] are much needed for many optical devices such as fiber sensors [4], fiber lasers [5], optical amplifiers [6], and fiber-based gyroscopes [7]. Although several designs in the past have achieved high-birefringence and single-polarization in solid-core [8] and photonic band gap [9] fibers, hollow-core anti-resonant fibers (HC-ARFs) have proven to be the foremost choice because of their unique and exceptional optical guidance in air [10]. HC-ARFs guide

light through inhibited-coupling between the core and cladding modes (CMs) and anti-resonant effect [11]. This mechanism provides wide transmission bandwidth [12], [13], [14], [15], [16], [17], [18], [19], extremely low power overlap with cladding tubes [20], low anomalous dispersion [21] and ultra-low loss [22].

Achieving high-birefringence and single-polarization using the HC-ARF structure is a relatively new concept, which was first proposed in 2016 [23]. Recently, a few high-birefringence and single-polarization HC-ARF designs have been proposed in the near-IR regime mostly at 1550 nm or 1064 nm with different cladding arrangements and number of layers in the cladding structure [23], [24], [25], [26]. High-birefringence and single-polarization were achieved either by using multiple nested resonators [23], [26] or high-index materials (HIMs) in the cladding [24]. A recent investigation has focused on examining a nested HC-ARF design that exhibits complexity and anisotropic properties. This study aims to achieve low loss and single-polarization specifically at the wavelength of 1550 nm, as highlighted in [27]. Most recently, a four-fold [26] and six-fold [28] symmetry bi-thickness HC-ARF were experimentally reported with outstanding optical performances. For example, in [26], a phase birefringence of 2.35×10^{-5} and 9.1×10^{-5} at 1550 and 1589 nm were achieved respectively.

To the best of our knowledge, the exploration of single-polarization and single-mode HC-ARF at a wavelength of $2 \mu\text{m}$ has not been conducted. In this paper, we introduce a novel nested HC-ARF having all circular tube design that incorporates a hybrid cladding of silica and HIM. The proposed design aims to achieve simultaneous benefits such as low propagation loss, single-polarization characteristics, high birefringence, and endlessly single-mode operation at $2 \mu\text{m}$ wavelength for applications such as fiber sensors, fiber lasers, and fiber-based gyroscopes.

The article is structured as follows: Section II presents the proposed fiber architecture. The selection of HIM material is outlined in Section III. Section IV provides a detailed description of the numerical results and discussions, encompassing comprehensive optimization procedures, single-mode operation, suppression of higher-order modes, and analysis of bend losses. The future investigations on random fiber imperfections is outlined in Section V. Section VI summarizes this article with an emphasize on investigating single-polarization HC-ARF at $2 \mu\text{m}$ wavelength.

Manuscript received 20 February 2024; revised 11 March 2024; accepted 17 March 2024. Date of publication 20 March 2024; date of current version 18 April 2024. The work of Md. Selim Habib was supported by the Woodrow W. Everett, Jr. SCEEE Development Fund in cooperation with the Southeastern Association of Electrical Engineering Department Heads. (*Corresponding author: Md. Selim Habib.*)

Herschel Herring is with the Department of Electrical and Computer Engineering, Florida Polytechnic University, Lakeland, FL 33805 USA (e-mail: hherring2105@floridapoly.edu).

Mohammad Al Mahfuz and Md. Selim Habib are with the Department of Electrical Engineering and Computer Science, Florida Institute of Technology, Melbourne, FL 32901 USA (e-mail: mmahfuz2024@my.fit.edu; mhabib@fit.edu).

Digital Object Identifier 10.1109/JPHOT.2024.3379478

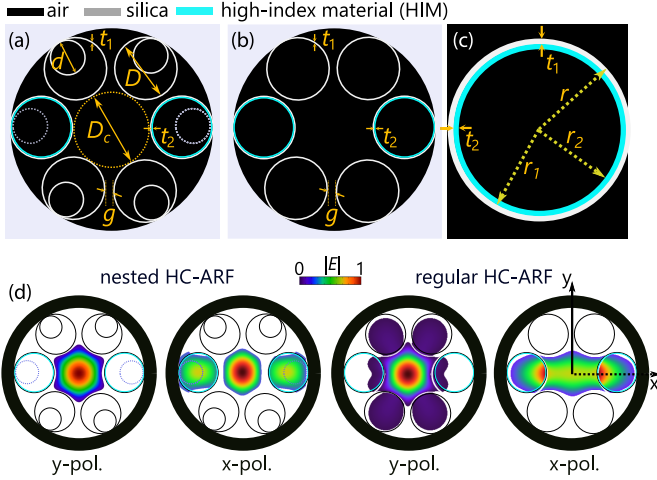


Fig. 1. HC-ARF geometries: 6-tube (a) nested HC-ARF and (b) regular HC-ARF in which the nested tubes are not present in the outer tubes. (c) Magnification of the outer tube indicating the wall thickness of silica/HIM tubes, radius of outer/external/inner tube, $r/r_1/r_2$. Both fibers have a core diameter of $D_c = 56 \mu\text{m}$, $t_1/t_2 =$ wall thickness of silica/HIM tubes, $d =$ nested tube diameter, $D =$ outer tube diameter, and $g =$ separation between the outer tubes. (d) Normalized mode-field profiles of both polarizations for nested and regular HC-ARF at $2 \mu\text{m}$. The color bar shows the intensity distributions in a linear scale. The mode-field profile (y -polarization) of nested HC-ARF is more confined to the core compared to the regular HC-ARF.

II. FIBER GEOMETRY

The HC-ARF geometries investigated in this work are displayed in Fig. 1(a)–1(b). In Fig. 1(a), we present an architecture of a nested non-touching all circular tube HC-ARF. The design incorporates high-index material (HIM) tubes (depicted in cyan color) inserted into two horizontally positioned silica tubes. This arrangement aims to achieve low loss specifically for one polarization state (y -polarization), while inducing high loss for the other polarization state (x -polarization). The HC-ARF has core diameter of D_c , tube diameter D , wall thickness of silica/HIM tubes, t_1/t_2 , nested tube ratio, d/D , and a gap separation between the outer tubes, g . Fig. 1(b) shows a regular HC-ARF design without nested tubes. In all our simulations, we choose a relatively large core diameter of $D_c = 56 \mu\text{m}$ to ensure low loss in the y -polarization. However, we optimize the silica/HIM tube thickness (t_1/t_2), and gap separation, g to ensure single-polarization, single-mode, and high-birefringence. The outer diameter D is related to the core diameter D_c , wall thickness t_1 , and number of tubes N , which can be written as [29]:

$$\frac{D}{2} = \frac{\frac{D_c}{2} \sin(\frac{\pi}{N}) - \frac{g}{2} - t_1(1 - \sin(\frac{\pi}{N}))}{1 - \sin(\frac{\pi}{N})}. \quad (1)$$

In all of our simulations, we took into account a common scenario found in fabricated fibers, where a small portion (represented as $t_1/2$) of the cladding tubes penetrates the outer silica tube [30].

III. SELECTION OF HIM

Identifying a high-index material (HIM) with low loss that exhibits both high birefringence and single-polarization at $2 \mu\text{m}$

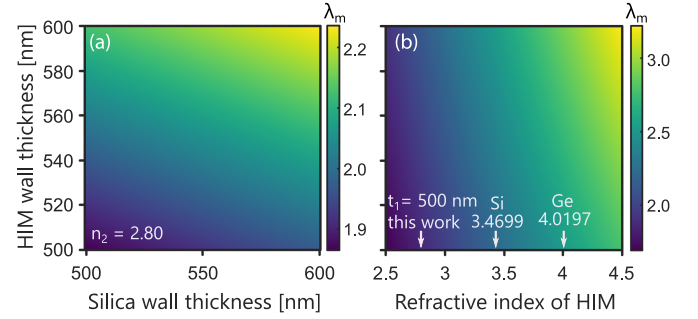


Fig. 2. Calculated resonance wavelength, λ_m (a) as a function of HIM thickness, t_2 with different values of silica thickness, t_1 for a fixed HIM refractive index of $n_2 = 2.80$ and (b) as a function of HIM thickness, t_2 with different refractive index of HIM for a fixed silica wall thickness, $t_1 = 500 \text{ nm}$. The simulations are calculated for a fixed core diameter $D_c = 56 \mu\text{m}$ and gap separation, $g = 2 \mu\text{m}$. The refractive indices of this work, Silicon (Si) [31], and Germanium (Ge) [32] are indicated by arrows in (b).

wavelength can be quite challenging. In this particular study, we have chosen a HIM with a refractive index of 2.80 (Chalcogenide). However, it is important to note that alternative HIMs, such as Silicon (Si) [33], Germanium (Ge) [32], and compound materials [34], could also be considered viable options, as long as they are accompanied by suitable t_1/t_2 values. The resonance wavelength of y -polarization (corresponds to high loss) depends on the refractive index of HIM and wall thickness of t_1/t_2 , which can be approximated using [12], [35]:

$$\lambda_m = \frac{2t_{\text{eq}} \sqrt{n_{\text{eq}}^2 - 1}}{m}, \quad m = 1, 2, 3, \dots \quad (2)$$

where m is the resonance order, and $t_{\text{eq}} = t_1 + t_2$.

The equivalent refractive index, n_{eq} is calculated using [34]:

$$n_{\text{eq}} = n_1 \frac{A_1}{A_1 + A_2} + n_2 \frac{A_2}{A_1 + A_2}, \quad (3)$$

where n_1 and n_2 are the refractive index of silica and HIM respectively, and A_1 and A_2 are the surface areas of two materials given by:

$$A_1 = \pi (r^2 - r_1^2); \quad A_2 = \pi (r_1^2 - r_2^2), \quad (4)$$

where r is the radius of outer tubes, r_1 and r_2 are the external and internal tube radius of the HIM. The equivalent refractive index, n_{eq} is a function of n_1 and n_2 and surface areas of two materials. It can be seen from (2) that for a given refractive index and wall thickness of HIM, the resonance wavelength for x -polarization can be determined or vice versa. The calculated resonance wavelength for x -polarization as a function of HIM wall thickness, t_2 for (a) different values of silica wall thickness, t_1 for a fixed value of HIM refractive index and (b) different values of HIM refractive index with a fixed silica wall thickness, t_1 is displayed in Fig. 2. The results displayed in Fig. 2 will provide initial guidelines to estimate t_1/t_2 values for a fixed HIM refractive index and t_2 values for a fixed t_1 and n_1 values. Nevertheless, to obtain precise predictions for the ratios of t_1/t_2 , finite-element (FE) modeling is necessary.

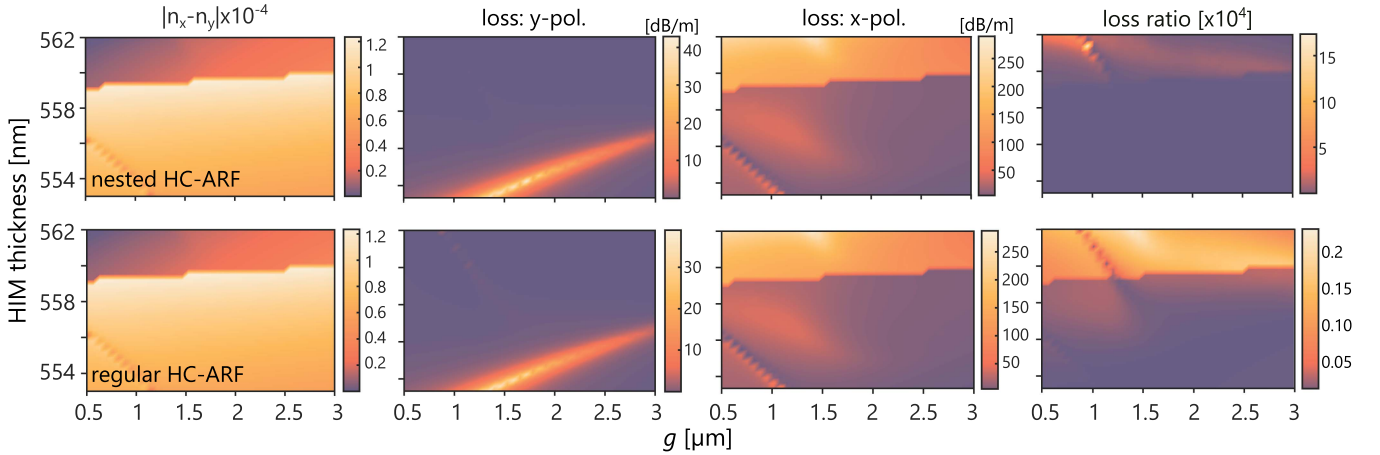


Fig. 3. FE-simulated results of birefringence: $|n_x - n_y|$, propagation loss in dB/m of y and x -polarizations, and PER or loss ratio of both polarizations. Top panel: nested HC-ARF, and bottom panel: regular HC-ARF. The HC-ARF has core diameter, $D_c = 56 \mu\text{m}$, normalized tube ratio, $d/D = 0.5$, and $t_1/t_2 = 564/559 \text{ nm}$. The simulations were performed at $2 \mu\text{m}$. To depict the 2D surface plots, gap separation, g , and HIM wall thickness, t_2 were scanned with 30 and 40 data points respectively and between the data points are interpolated.

IV. NUMERICAL RESULTS AND DISCUSSION

The simulations were performed using fully-vectorial FE modeling. A perfectly-matched layer (PML) boundary was placed outside the fiber domain to accurately calculate the confinement loss. The mesh size and PML boundary conditions were chosen similar to [12], [25], [36]. The propagation loss was calculated by considering confinement loss, effective material loss [36], and surface scattering loss (SSL) [12], [37].

A. Optimization of Gap Separation and HIM Wall Thickness

We started our investigations towards achieving high-birefringence, single-mode, and single-polarization by optimizing the gap separation, g and the HIM wall thickness, t_2 for a fixed core diameter, $D_c = 56 \mu\text{m}$, silica wall thickness, $t_1 = 560 \text{ nm}$, and normalized nested tube ratio, $d/D = 0.5$. The desired properties of low loss, single-polarization, and high-birefringence are highly dependent on these two parameters. In particular, the effect of g is critical to examine since it heavily influences how the fundamental-mode (FM) of one polarization is guided in the core while that of the other polarization spreads to the cladding. Fig. 1(d) shows the mode-field profiles of both nested and regular HC-ARFs in which it can be seen that the light of y -polarization is almost entirely guided in the core, while the light of x -polarization spreads more towards the HIM cladding. It is also clear that there is enhanced performance with the nested HC-ARF compared to regular HC-ARF as more of the light is well guided in the core and weakly leaks towards the cladding.

The FE-simulated results for nested and regular HC-ARF are shown in Fig. 3. From the 2D surface plots, we can see that there is low loss for y -polarization, high loss for x -polarization, high-birefringence, and high loss ratio around the region where $g = 2 \mu\text{m}$ and $t_2 = 559 \text{ nm}$. The graphical patterns for the nested and regular HC-ARF are similar in regards to birefringence and the loss of both polarizations, however, the nested structure displays a much higher loss ratio. Numerically, the nested structure also shows significantly lower loss of the y -polarization with

a minimum FM loss of $\approx 0.0011 \text{ dB/m}$ comparing to that of the regular structure at $\approx 0.05 \text{ dB/m}$. It is also evident that the ideal range is more highly impacted by the value of the HIM wall thickness, since there is a visible boundary near $t_2 = 559 \text{ nm}$ where the birefringence drops greatly from $> 1.23 \times 10^{-4}$ to $< 0.27 \times 10^{-4}$. For both nested and regular HC-ARFs, the maximum possible loss of x -polarization, birefringence, and loss ratio as well as the minimum loss of the y -polarization do not all occur at the same values of g and t_2 . For example, the nested structure's best values are 290 dB/m , $> 1.23 \times 10^{-4}$, $> 1.7 \times 10^5$, and $\approx 1 \text{ dB/km}$ respectively, and all occurring for different values of g and t_2 . The optimum region where high-birefringence of $> 1.0 \times 10^{-4}$ is achieved while maintaining an FM loss of the y -polarization of $< 0.05 \text{ dB/m}$ is highly sensitive, and occurs where $g = 2 \mu\text{m}$ and $559 \text{ nm} < t_2 < 559.5 \text{ nm}$. A polarization-extinction ratio (PER) or loss ratio of > 550 is shown in this region as well. Values near this t_2 range were chosen for analysis in further sections with the anticipation that high-birefringence, low loss, and single-mode operation could be enhanced with additional parameter tuning.

B. Optimization of silica/HIM Wall Thickness (t_1/t_2)

In this section, we optimized the wall thicknesses of silica/HIM, while fixing our gap separation, $g = 2 \mu\text{m}$ as found in the previous section. Here, we maintained the fixed core diameter and normalized nested tube ratio of $D_c = 56 \mu\text{m}$ and $d/D = 0.5$, respectively. From the results of the 2D contour plots seen in Fig. 4, we can see that the wall thicknesses are crucial to achieving low loss, high-birefringence, and single-polarization. As mentioned previously, we chose the value of $g = 2 \mu\text{m}$ with the anticipation that further parameter tuning could lead to enhanced birefringence. From the simulated results of the silica/HIM sweep, high-birefringence of $> 1.20 \times 10^{-4}$ was achieved in the region where $t_1 = 564 \text{ nm}$ and $t_2 = 559 \text{ nm}$. At these values, the FM loss of the y -polarization can be made as low as 0.02 dB/m while the loss of the x -polarization is

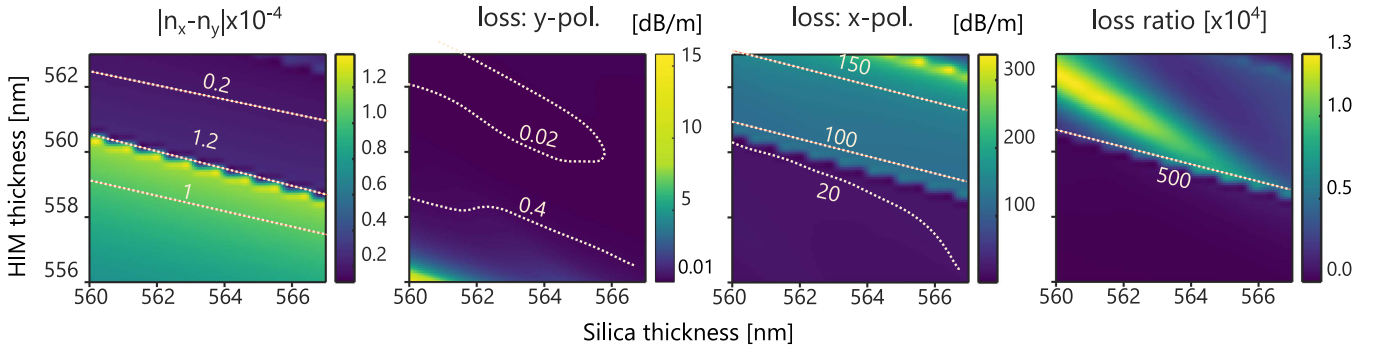


Fig. 4. FE-simulated results of birefringence: $|n_x - n_y|$, propagation loss of y and x -polarizations, and loss ratio of both polarizations as a function of HIM thickness, t_2 with different values of silica thickness, t_1 . The HC-ARF has core diameter, $D_c = 56 \mu\text{m}$, normalized tube ratio, $d/D = 0.5$, and gap separation, $g = 2 \mu\text{m}$. The simulations were performed at $2 \mu\text{m}$. Silica wall thickness, t_1 , and HIM wall thickness, t_2 were scanned with 25 and 30 data points respectively and between the data points are interpolated.

>20 dB/m. The loss ratio is in the range of 578-970 here as well. Again, the birefringence is highly sensitive to changes in the wall thickness of HIM and a sharp drop can be seen once it exceeds 559 nm. These results demonstrate that by sufficient tuning of the silica thickness t_1 , we are able to enhance the properties of low loss, high-birefringence, and single-polarization. By doing so, we were able to increase high-birefringence from $>1.0 \times 10^{-4}$ to $>1.2 \times 10^{-4}$ and loss ratio from >400 to >550 while reducing the FM loss of the y -polarization from <0.05 dB/m to <0.03 dB/m.

C. Single-Mode Operation and Higher-Order Mode Suppression

Following the examination of the low loss, high-birefringence, and single-polarization, the effectively single-mode operation and the suppression of the higher-order modes (HOMs) is demonstrated by optimization of the gap separation, g , and the nested tube ratio, d/D . The FE-simulated results for this are shown in Fig. 5, where we can easily see that there is a large region where the loss of the FM is very low (<0.02 dB/m) while the loss of the HOMs is high (>20 dB/m). It is also important to note that FM loss is more heavily influenced by changes in g compared to changes in d/D . However, d/D has a significant impact on the loss of the HOMs. The region of highest loss of the HOMs becomes narrow for the range $1 \mu\text{m} < g < 2.5 \mu\text{m}$, where the value of d/D must be precise in order to obtain effectively single-mode operation. The coupling between the core-guided HOMs and CMs is shown in Fig. 5(c)-(d). The effective mode index of the FM-like mode (red dotted line) remains unchanged as a function of d/D , avoiding any phase matching with CMs. This mechanism confirms low loss guidance. However, the effective index of HOMs strongly couple with CMs and tube modes at various values of d/D (also see Fig. 5(d)), ensuring high loss for HOMs, thus confirming effective single-mode operation.

D. Core Diameter Optimization

Next, we investigated the effect of changing the core diameter D_c on the FM loss of both polarizations for a fixed

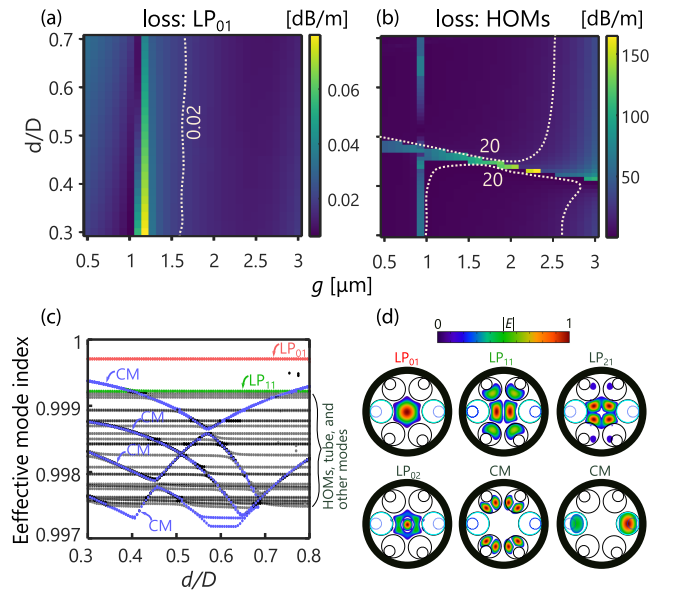


Fig. 5. FE-simulated propagation loss of y -polarization for (a) LP_{01} -mode and (b) HOMs for varying values of d/D and gap separation, g . Results were scanned with 50 and 30 data points respectively and between the data points are interpolated. Effect of changing normalized nested tube ratio, d/D on (c) Effective mode index with a core diameter, $D_c = 56 \mu\text{m}$, $t_1/t_2 = 564/559$ nm, and gap separation, $g = 2 \mu\text{m}$. The normalized tube ratio, d/D were scanned from 0.3 to 0.8 by simulating 50 modes at $2 \mu\text{m}$. (d) The electric field intensities of the first four core-guided modes and CMs are shown for $d/D \approx 0.42$ and $g = 2 \mu\text{m}$ on a linear color scale.

$g = 2 \mu\text{m}$, silica wall thickness, $t_1/t_2 = 564/559$ nm, and normalized nested tube ratio, $d/D = 0.5$. The results of the core diameter analysis in Fig. 6(a) revealed that the loss of the y -polarization remains low and relatively unchanged for all values while the loss of the x -polarization is significantly higher yet decreasing with the core diameter. For our previous analyses, we fixed the core diameter $D_c = 56 \mu\text{m}$, however, we saw that the FM of the x -polarization can be made more lossy for lower core diameter values around 50–52 μm . There is strong high-birefringence in this region of $>1.48 \times 10^{-4}$, however, the loss of the y -polarization increases to >0.1 dB/m at $D_c = 50 \mu\text{m}$ specifically, as shown in Fig. 6(b). Since high-birefringence

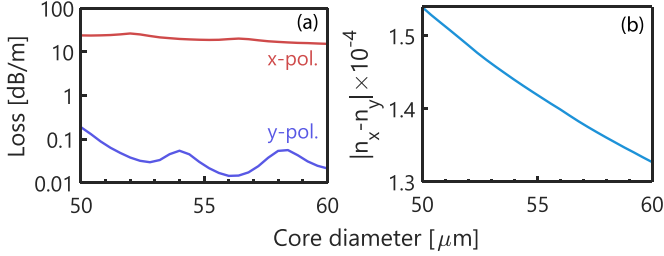


Fig. 6. FE-simulated (a) propagation loss of both polarization for LP_{01} -mode and (b) birefringence for different values of core diameters. The HC-ARF has silica/HIM wall thickness, $t_1/t_2 = 564/559$ nm, gap separation, $d/D = 0.5$, and $g = 2$ μm . The simulations were performed at 2 μm .

of $>1.3 \times 10^{-4}$ is achieved for any value of D_c , an optimum region can be determined simply by where the loss of the y -polarization is the lowest. This occurs in the range of 55.6 $\mu\text{m} < D_c < 56.8$ μm , where the FM loss of the y -polarization remains <0.2 dB/m. Thus we have shown that by changing the core diameter D_c , we can achieve even better performance in regards to low loss, high-birefringence, and single-polarization.

E. Bend Loss Analysis

Lastly, we examined the bend loss of nested HC-ARF for a range of bend radii R_b of 5 – 10 cm for different $g = \{2, 3, 4\}$ μm , fixed core diameter $D_c = 56$ μm , $t_1/t_2 = 564/559$ nm, and normalized nested tube ratio, $d/D = 0.65$. We utilize the standard conformal transformation to alter the refractive index of a comparable straight fiber in order to determine the bend loss of the fibers [38], [39]: $n_b = n(x, y)e^{(x, y)/R_b}$, where R_b is the bend radius, x is the bend direction, $n(x, y)$ is the refractive index profile of the straight fiber and n_b is the equivalent refractive index after bending. The bend loss of x -direction is much higher than y -direction and has strong light coupling to the tube modes as expected due to the missing nested tubes in the x -directions. The strong coupling between the core modes and tubes modes occur at different bend radii and the coupling shifts for different g values. This phenomenon is interesting because it indicates that the fiber can be used as a polarization filter at those gap separations and bend conditions as displayed in Fig. 7.

V. FUTURE INVESTIGATIONS

This study focuses exclusively on an ideal HC-ARF structure, where key parameters such as tube gap separations (g) and wall thicknesses of silica/HIM (t_1/t_2) remain constant. Additionally, the cladding tubes are assumed to have a circular shape, as depicted in Fig. 8(a). However, in practice, random structural perturbations, including fluctuations in tube wall thicknesses, tube gap separations, anisotropic nested and outer tubes which commonly occur during fiber fabrication (see Fig. 8(b)), were not taken into account. These variations may have the potential to influence the overall loss, polarization properties, and single-mode propagation performance. Hence, it is inevitable to encounter these effects and we will investigate these effects on the overall performance of the proposed HC-ARF in future.

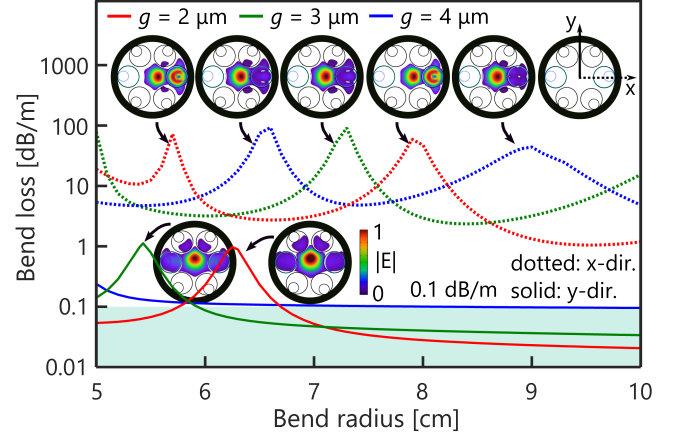


Fig. 7. Calculated bend loss of both polarizations versus bend radius from 5 cm to 10 cm in steps of 0.1 cm for different gap separations for x and y -bend directions. The HC-ARF has core diameter, $D_c = 56$ μm , silica/HIM wall thickness, $t_1/t_2 = 564/559$ nm, gap separation, $d/D = 0.65$, and $g = 2$ μm (red), 3 μm (green), and 4 μm (blue). The simulations were performed at 2 μm . The high loss peaks can be used for polarization filters. Inset: the electric field intensities on a linear color scale are shown for different bend radii.

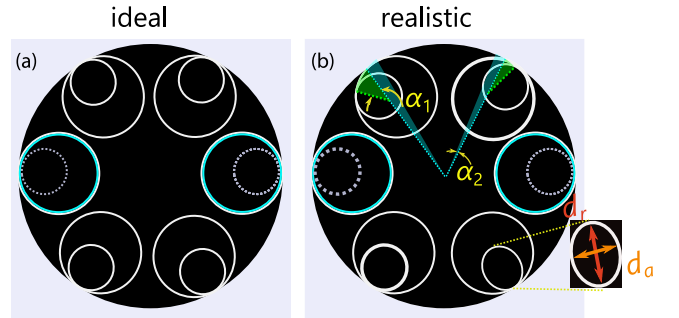


Fig. 8. (a) Ideal circular cladding tube HC-ARF architecture with constant tube gap separations, g and wall thickness of silica/HIM, t_1/t_2 . (b) Realistic HC-ARF design with random wall thicknesses, tube gap separations, and anisotropic tube shapes. The tube offset angles are denoted by $\alpha_1, \alpha_2, \dots, \alpha_n$.

VI. CONCLUSION

In conclusion, we present a HC-ARF architecture that has been developed and validated to have single-polarization, high-birefringence, and single-mode operation characteristics at the 2 μm wavelength. Through extensive fiber parameter optimizations based on regular and nested hybrid silica/HIM HC-ARF structures, we demonstrated that the nested geometry has better performance compared to regular HC-ARF. We also found a favorable range of the gap separation and HIM wall thickness. From there, we were able to tune the silica thickness to obtain enhanced low loss, high-birefringence, and polarization-extinction ratio of 0.02 dB/m, 1.2×10^{-4} , and >550 , respectively. Furthermore, effectively single-mode operation was achieved by suitably choosing the nested tube ratio, d/D . We found that the loss of the HOMs could be made as high as 20 dB/m while the loss of the FM was <0.02 dB/m for a large range of g and d/D values. Finally, we investigated the effect of changing the bend radius in both x and y -directions. We found that FM bend loss for x -direction was much higher than the y -direction due to

the strong light coupling to the tube modes. The strong coupling between the core-guided modes and CMs lead to an interesting phenomenon through which the proposed fiber can be used as polarization filter. The exceptional polarization, low propagation loss, and single-mode properties presented in this work will pave the way toward practical applications at the highly appealing 2 μm wavelength.

REFERENCES

- [1] K. Scholle, S. Lamrini, P. Koopmann, and P. Fuhrberg, "2 μm laser sources and their possible applications," in *Frontiers in Guided Wave Optics and Optoelectronics*. Rijeka, Croatia: IntechOpen, 2010.
- [2] S. B. Mirov, V. V. Fedorov, D. Martyskhin, I. S. Moskalev, M. Mirov, and S. Vasilyev, "Progress in mid-IR lasers based on CR and Fe-doped II-VI chalcogenides," *IEEE J. Sel. Topics Quantum Electron.*, vol. 21, no. 1, pp. 292–310, Jan.-Feb., 2015.
- [3] A. Taranta et al., "Exceptional polarization purity in antiresonant hollow-core optical fibres," *Nature Photon.*, vol. 14, no. 8, pp. 504–510, 2020.
- [4] S. Chen et al., "Local electric field enhancement and polarization effects in a surface-enhanced Raman scattering fiber sensor with chessboard nanostructure," *Opt. Exp.*, vol. 16, no. 17, pp. 13016–13023, 2008.
- [5] J. T. Lin and W. A. Gambling, "Polarisation effects in fibre lasers: Phenomena, theory and applications," in *Proc. IEE Colloq. Polarisation Effects Opt. Switching Routing Syst.*, 1990, pp. 10/1–10/3.
- [6] X. Peng and L. Dong, "Fundamental-mode operation in polarization-maintaining ytterbium-doped fiber with an effective area of 1400 μm^2 ," *Opt. Lett.*, vol. 32, no. 4, pp. 358–360, 2007.
- [7] M. A. Terrel, M. J. F. Digonnet, and S. Fan, "Resonant fiber optic gyroscope using an air-core fiber," *J. Lightw. Technol.*, vol. 30, no. 7, pp. 931–937, Apr. 2012.
- [8] T. Hosaka, K. Okamoto, T. Miya, Y. Sasaki, and T. Eda, "Low-loss single polarisation fibres with asymmetrical strain birefringence," *Electron. Lett.*, vol. 17, no. 15, pp. 530–531, 1981.
- [9] J. M. Fini et al., "Polarization maintaining single-mode low-loss hollow-core fibers," *Nature Commun.*, vol. 5, no. 1, 2014, Art. no. 5085.
- [10] H. Sakr et al., "Hollow core optical fibres with comparable attenuation to silica fibres between 600 and 1100 nm," *Nature Commun.*, vol. 11, no. 1, pp. 1–10, 2020.
- [11] F. Couny, F. Benabid, P. Roberts, P. Light, and M. Raymer, "Generation and photonic guidance of multi-octave optical-frequency combs," *Science*, vol. 318, no. 5853, pp. 1118–1121, 2007.
- [12] F. Poletti, "Nested antiresonant nodeless hollow core fiber," *Opt. Exp.*, vol. 22, no. 20, pp. 23807–23828, 2014.
- [13] P. Uebel et al., "Broadband robustly single-mode hollow-core PCF by resonant filtering of higher-order modes," *Opt. Lett.*, vol. 41, no. 9, pp. 1961–1964, 2016.
- [14] M. S. Habib et al., "Low-loss single-mode hollow-core fiber with anisotropic anti-resonant elements," *Opt. Exp.*, vol. 24, no. 8, pp. 8429–8436, 2016.
- [15] B. Debord et al., "Ultralow transmission loss in inhibited-coupling guiding hollow fibers," *Optica*, vol. 4, no. 2, pp. 209–217, 2017.
- [16] S.-F. Gao et al., "Hollow-core conjoined-tube negative-curvature fibre with ultralow loss," *Nature Commun.*, vol. 9, no. 1, pp. 1–6, 2018.
- [17] W. Ding, Y.-Y. Wang, S.-F. Gao, M.-L. Wang, and P. Wang, "Recent progress in low-loss hollow-core anti-resonant fibers and their applications," *IEEE J. Sel. Topics Quantum Electron.*, vol. 26, no. 4, Jul./Aug., 2020, Art. no. 4400312.
- [18] A. I. Adamu et al., "Deep-UV to mid-IR supercontinuum generation driven by mid-IR ultrashort pulses in a gas-filled hollow-core fiber," *Sci. Rep.*, vol. 9, no. 1, pp. 1–9, 2019.
- [19] M. Cooper et al., "2.2 kW single-mode narrow-linewidth laser delivery through a hollow-core fiber," *Optica*, vol. 10, no. 10, pp. 1253–1259, 2023.
- [20] M. Michieletto et al., "Hollow-core fibers for high power pulse delivery," *Opt. Exp.*, vol. 24, no. 7, pp. 7103–7119, 2016.
- [21] H. Sakr et al., "Interband short reach data transmission in ultrawide bandwidth hollow core fiber," *J. Lightw. Technol.*, vol. 38, no. 1, pp. 159–165, Jan. 2020.
- [22] G. T. Jason et al., "0.174 dB/km hollow core double nested antiresonant nodeless fiber (DNANF)," in *Proc. Opt. Fiber Commun. Conf. Exhib.*, 2022, pp. 1–3.
- [23] S. A. Mousavi, S. R. Sandoghchi, D. J. Richardson, and F. Poletti, "Broadband high birefringence and polarizing hollow core antiresonant fibers," *Opt. Exp.*, vol. 24, no. 20, pp. 22943–22958, 2016.
- [24] S. Yan, Z. Lian, S. Lou, X. Wang, W. Zhang, and Z. Tang, "A new method to achieve single-polarization guidance in hollow-core negative-curvature fibers," *IEEE Access*, vol. 8, pp. 53419–53426, 2020.
- [25] M. S. Habib, A. Adamu, C. Markos, and R. Amezcua-Correa, "Enhanced birefringence in conventional and hybrid anti-resonant hollow-core fibers," *Opt. Exp.*, vol. 29, no. 8, pp. 12516–12530, 2021.
- [26] Y.-F. Hong et al., "Highly birefringent anti-resonant hollow-core fiber with a bi-thickness fourfold semi-tube structure," *Laser Photon. Rev.*, vol. 16, no. 5, 2022, Art. no. 2100365.
- [27] M. S. Hosen et al., "Highly birefringent polarization maintaining low-loss single-mode hollow-core antiresonant fiber," *Opt. Continuum*, vol. 1, no. 10, pp. 2167–2184, 2022.
- [28] S. Yerolatsitis, R. Shurvinton, P. Song, Y. Zhang, R. J. A. Francis Jones, and K. R. Rusimova, "Birefringent anti-resonant hollow-core fiber," *J. Lightw. Technol.*, vol. 38, no. 18, pp. 5157–5162, Sep. 2020.
- [29] C. Wei, R. J. Weiblen, C. R. Menyuk, and J. Hu, "Negative curvature fibers," *Adv. Opt. Photon.*, vol. 9, no. 3, pp. 504–561, 2017.
- [30] W. Belardi and J. C. Knight, "Hollow antiresonant fibers with low bending loss," *Opt. Exp.*, vol. 22, no. 8, pp. 10091–10096, 2014.
- [31] E. Shkondin et al., "Large-scale high aspect ratio Al-doped ZnO nanopillars arrays as anisotropic metamaterials," *Opt. Mater. Exp.*, vol. 7, no. 5, pp. 1606–1627, 2017.
- [32] H. Li, "Refractive index of silicon and germanium and its wavelength and temperature derivatives," *J. Phys. Chem. Reference Data*, vol. 9, no. 3, pp. 561–658, 1980.
- [33] C. Schinke et al., "Uncertainty analysis for the coefficient of band-to-band absorption of crystalline silicon," *AIP Adv.*, vol. 5, no. 6, 2015, Art. no. 067168.
- [34] W. Belardi, F. D. Lucia, F. Poletti, and P. J. Sazio, "Composite material hollow antiresonant fibers," *Opt. Lett.*, vol. 42, no. 13, pp. 2535–2538, 2017.
- [35] M. Duguay, Y. Kokubun, T. Koch, and L. Pfeiffer, "Antiresonant reflecting optical waveguides in SiO₂-Si multilayer structures," *Appl. Phys. Lett.*, vol. 49, no. 1, pp. 13–15, 1986.
- [36] M. S. Habib, J. Antonio-Lopez, C. Markos, A. Schülzgen, and R. Amezcua-Correa, "Single-mode, low loss hollow-core anti-resonant fiber designs," *Opt. Exp.*, vol. 27, no. 4, pp. 3824–3836, 2019.
- [37] P. Roberts et al., "Ultimate low loss of hollow-core photonic crystal fibres," *Opt. Exp.*, vol. 13, no. 1, pp. 236–244, 2005.
- [38] M. Heiblum and J. Harris, "Analysis of curved optical waveguides by conformal transformation," *IEEE J. Quantum Electron.*, vol. JQE-11, no. 2, pp. 75–83, Feb. 1975.
- [39] M. H. Frosz, P. Roth, M. C. Günendi, and P. S. J. Russell, "Analytical formulation for the bend loss in single-ring hollow-core photonic crystal fibers," *Photon. Res.*, vol. 5, no. 2, pp. 88–91, 2017.